Eddy covariance flux measurements of gaseous elemental mercury using cavity ring-down spectroscopy

Ashley M. Pierce†[1], Christopher W. Moore[1], Georg Wohlfahrt[2], Lukas Hörtnagl[2], Natascha Kljun[3], Daniel Obrist[1]*

[1]Desert Research Institute, Division of Atmospheric Sciences, Reno, NV, USA

[2]University of Innsbruck, Institute of Ecology, Innsbruck, Austria

[3]Swansea University, Department of Geography, Swansea, UK

Keywords: Eddy covariance flux measurements, gaseous elemental mercury (GEM), pulsed cavity ring-down spectroscopy (CRDS), modified Bowen ratio, dynamic flux chamber

15 Abstract

16 A pulsed cavity ring-down spectroscopy (CRDS) system for measuring atmospheric
17 gaseous elemental mercury (GEM) concentrations at high temporal resolution was used
18 to successfully conduct eddy covariance (EC) flux measurements of GEM. GEM fluxes
19 from soils are important to understand because they can originate from natural sources,
20 legacy emissions, and re-emission of previously deposited anthropogenic pollution,
21 which together exceed primary anthropogenic emissions. Eddy covariance flux
22 measurements require sub-second concentration measurements, hampering the
23 measurement of GEM fluxes due to slow response instrumentation. Measurements took
24 place near Reno, Nevada in September and October 2012 encompassing natural, low-
25 mercury (Hg) background soils and Hg-enriched soils. During nine days of measurements
26 with deployment of Hg-enriched soil in boxes within 60 m upwind of the EC tower, clear
27 covariance of GEM concentration and vertical wind speed was measured, showing that
28 EC fluxes over an Hg-enriched area were detectable. During three separate days of flux
29 measurements over background soils (without Hg-enriched soils), no covariance was
30 detected – indicating fluxes below the detection limit. When fluxes were measurable,
31 they strongly correlated with wind direction; and highest fluxes occurred when winds
32 originated from the Hg-enriched area. We also measured fluxes with the modified Bowen
33 ratio (MBR) and a dynamic flux chamber (DFC). Comparisons between the three
34 methods generally showed good agreement in direction (e.g., emission or deposition) and
35 magnitude of fluxes measured, in particular when measured fluxes originated from within
36 the area of Hg-enriched soils. This study demonstrated that a CRDS system can be used

to measure GEM fluxes over Hg-enriched areas, with a conservative detection limit estimate of 32 ng m^{-2} hr^{-1}, equivalent to the lowest measured absolute flux.

Introduction

Long-range atmospheric transport and deposition contributes to significant environmental mercury (Hg) loading even in remote ecosystems[1-3]. Large uncertainties remain in our understanding of deposition processes, in particular of gas-phase dry deposition which contributes significantly to deposition loads[4]. Gaseous elemental mercury (GEM), the dominant atmospheric form of Hg, is semi-volatile and subject to atmospheric deposition and re-emission leading to a complex pattern of net Hg surface-atmosphere exchange[4-6]. Processes contributing to GEM re-emission include photochemical reduction[7-10] as well as other abiotic and biotic processes[11-15]. Atmospheric GEM emissions from natural sources, legacy emissions, and re-emission of previously deposited anthropogenic pollution have been estimated to exceed primary anthropogenic emissions by a factor of four [16]. GEM is the dominant form of Hg in the atmosphere and is therefore the main pathway for Hg to enter ecosystems where it can then be methylated (MeHg) and become bioavailable. Once Hg becomes bioavailable it can bioaccumulate up the food web where it can reach concentrations in marine and terrestrial species known to cause health problem in wildlife and humans [17-19].

Several methods for measuring net GEM exchange between surfaces and the atmosphere have been employed, many of them have a number of shortcomings. The most widely used technique, the dynamic flux chamber (DFC), is an easy-to-deploy and relatively inexpensive method that is used to measure the exchange of GEM over a small area (usually <1 m^2). The DFC method is, however, highly sensitive to pressure differences and flow rates through the chamber[20]; and placement of the chamber also impacts ambient conditions such as temperature, radiation, humidity, and turbulence

64 levels[20-24]. Micrometeorological techniques, including the modified Bowen ratio (MBR),
65 aerodynamic and relaxed eddy accumulation methods, also have been used to measure
66 GEM fluxes[21, 25-31]. These methods can be used to measure surface fluxes in situ without
67 modification of environmental conditions, but have other limitations; in particular, the
68 MBR and aerodynamic methods assume equal transport characteristics for GEM and a
69 reference scalar (heat, water, or CO_2) to calculate fluxes (e.g., similarity theory) – which
70 is not always valid[32]. Another limitation is that concentration measurements are required
71 at two heights which may represent different source areas[33] or cause a bias due to the
72 time lag of alternating measurements between the two heights[26]. The relaxed eddy
73 accumulation method is a direct flux method, long sampling times are needed to acquire
74 enough sample volume to distinguish concentration differences between updrafts and
75 downdrafts[25, 34, 35].

76 Many of these issues could be overcome by using the eddy covariance (EC) technique
77 – the only known direct, in situ method of determining fluxes[36-38] and the current
78 standard for measuring atmospheric fluxes of many other trace gases (CO_2, methane,
79 ozone, and water vapor)[27, 36, 39]. The technique uses a sonic anemometer to measure high-
80 frequency eddies (small to large changes in vertical wind direction) and a suite of other
81 instruments to measure scalar atmospheric data to determine vertical turbulent fluxes and
82 therefore exchange rates of trace gases over a variety of landscapes and is useful for
83 assessing exchange over a whole ecosystem for hours to years[40]. This is done by
84 analyzing the covariance between the change in vertical wind speed from the mean (zero)
85 value and the change in a gas concentration (GEM) from its mean value[40, 41]. This
86 analysis allows for detailed spectral analyses of conditions and allows the operator to

qualify data as useable based on conditions favorable for micrometeorological measurements, which is not possible for other techniques discussed previously. Limitations of the EC method include the necessity for flat terrain, steady conditions but turbulent winds, and consistent vegetation[40]. EC measurements also require a fast-response (sub-second) field-deployable sensor, which until recently has not been available for GEM. To test the application of EC for GEM flux measurements, we deployed a newly developed pulsed cavity ring-down spectroscopy (CRDS) system[42, 43] capable of a measurement resolution of 25 Hz for GEM surface flux measurements with the EC technique. EC flux measurements were conducted over natural low-Hg background soils and over artificially Hg-enriched soil and compared to GEM fluxes measured with the MBR and DFC methods. The CRDS system was used to measure GEM concentrations at 25 Hz. These measurements were then averaged over half hour periods to calculate average GEM fluxes.

2. Methods

2.1 Field site

Measurements were performed from September 14 to October 1, 2012 at a site 32 km northeast of Reno, Nevada, USA (39° 41' N, 119° 32' W; elevation 1570 m) over a flat area (0.61 km^2) of mixed bare soil and shrubs in the Northern Desert Shrub Zone. Surrounding vegetation consisted mainly of sagebrush (*Artemisia tridentata*), rabbitbrush (*Ericameria nauseosa*), and juniper species (*Juniperus spp.)*, (Supp. Info. S1). The micrometeorological flux tower was located in the northwest corner of a 50 x 90 m^2 flat,

non-vegetated area with a small hill (elevation 35 m) starting 300 m to the southwest of the tower (Supp. Fig. S1a).

GEM flux measurements were first made at the site over soils with low background Hg concentrations (average soil Hg concentration: 0.11 ± 0.04 μg g^{-1}) from September 14 to 18, termed "background" measurements. From September 19 to September 29, plastic storage boxes containing Hg-enriched soil were deployed as additional GEM sources upwind, in the footprint area (cf. Section 2.4) of the micrometeorological towers, termed "Hg-enriched" measurements (Fig. 1a and Supp. Fig. S1). For this, 41 plastic storage boxes (58 cm x 41 cm) were deployed filled with a layer of Hg-enriched soil (average Hg concentration: 84.5 ± 5.25 μg g^{-1}) in a semi-circle around the micrometeorological towers (between 90˚ and 270˚ based on predominant wind direction in the area) equally spaced with 10 m between each box (Fig. 1a; Supp. Info. S.1). From September 29 to October 1, the boxes filled with Hg-enriched soil were removed for renewed background measurements (only atmospheric concentrations were measured, no fluxes). The sonic anemometer of the EC system was positioned, due to tower orientation, toward the south-southeast at an angle of 172° allowing unobstructed wind direction and ideal measurements from 82° to 262°, similar to the deployed Hg-enriched soil boxes (see Fig. 1a). All flux measurements were made between 12:00 and 18:00 Pacific Daylight Time, the time period when winds typically originated from the 90-270° sector (see Supp. Info. S.2, and Supp. Fig. S.2).

Figure 1

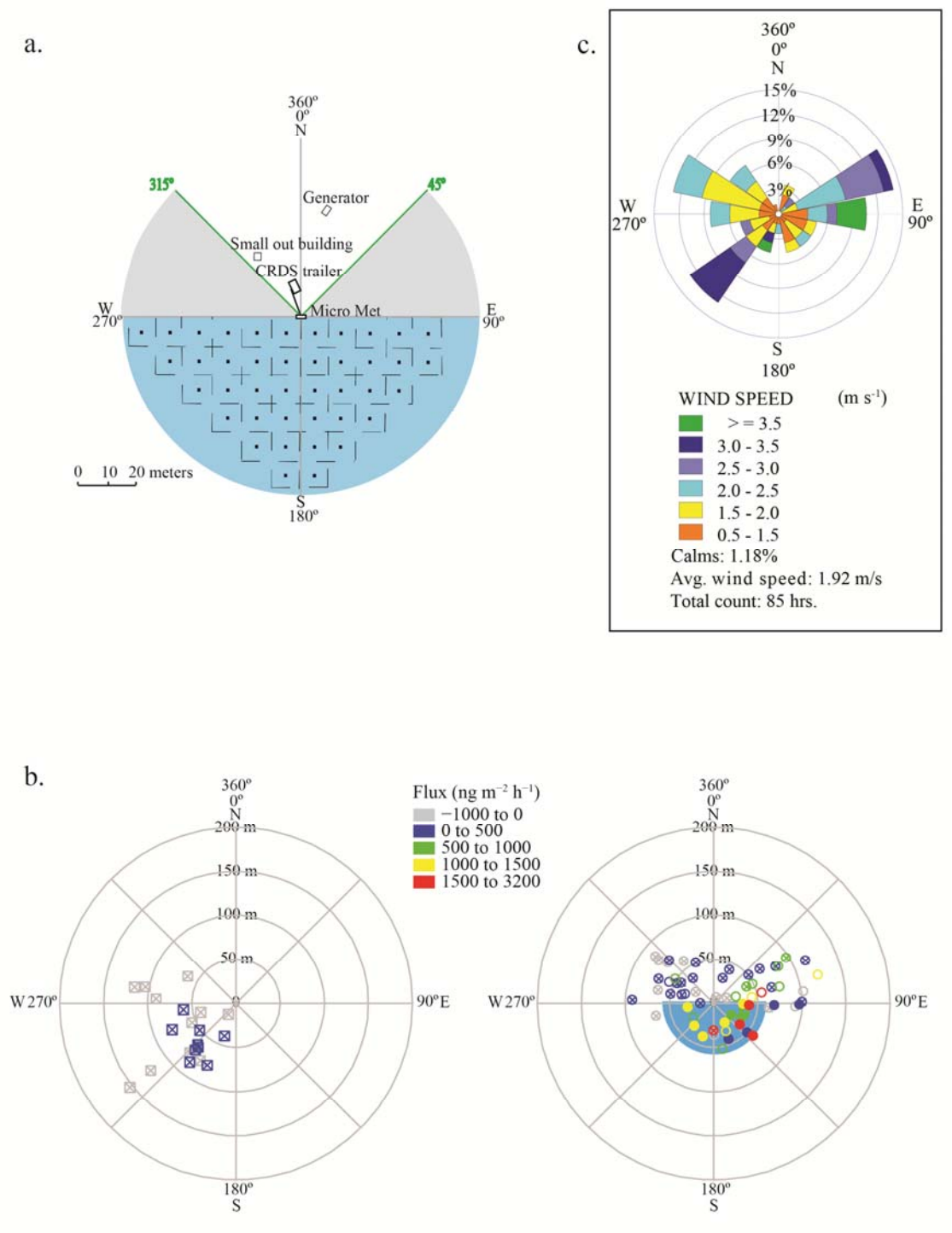

131

132

133 *2.2 Flux measurements*

2.2.1 Eddy covariance

Three measurement towers were deployed 10 m southeast of a trailer that contained the CRDS system[42, 43] and auxiliary analyzers. One tower supported a three-dimensional (3D) ultrasonic anemometer for measurement of the three wind components and the speed of sound (CSAT3, Campbell Scientific, Logan, UT, USA) mounted 75 cm above the ground along with an open-path infrared gas analyzer (IRGA, LI-7500, LiCor Inc. Lincoln, NE, USA) for CO_2 and water vapor concentration measurements (Supp. Info. S.3). The open-path IRGA and the air sampling inlet to measure GEM and ozone were mounted 20 cm below the center of the sensing volume of the sonic anemometer, with the IRGA positioned 10 cm east and 20 cm north of the air inlet. The air inlet was connected by 20 m Teflon® tubing (4.76 mm ID) to the mobile measurement trailer (Supp. Fig. S.1b). In addition, the sample air was routed through a set of glassware and ovens for ozone decomposition prior to measurements[42] and to the closed-path, 1 m quartz-coated stainless-steel measurement cavity of the CRDS system at a flow rate of 8 L min^{-1} for laminar flow (Reynolds number of ~1800). After the CRDS cavity, flow was distributed to an Hg vapor analyzer (Model 2537B, Tekran Inc., Toronto, Canada) which was used to correct CRDS GEM concentrations at 2.5 min time intervals, a closed-path IRGA (LI-7000, LiCor Inc.; Supp. Info. S.3), and an ozone analyzer (Model 205, 2B Technologies). The trailer also housed two additional Model 2537B analyzers to measure GEM concentrations for the MBR and DFC methods (see Supp. Info S.4).

2.2.2 Modified Bowed Ratio

In order to compare EC fluxes with other techniques, we also measured GEM fluxes with the MBR method. Since we were measuring in an arid environment, we chose to use sensible heat as the reference scalar for this technique. A third tower was used for the gradient setup where GEM concentrations and temperature were monitored at 0.58 and 1.09 m above the ground. Temperature at each height was continuously measured (1 min average) with two 1000 Ohm platinum resistance thermometers (PRTs; $\pm 0.01^{o}$ C; Thermometrics Corporation; Los Angeles, CA, USA). Each set of PRTs was placed in a fan-aspirated radiation shield (Model 076B; Met One Instruments; Grants Pass, OR, USA). Both heights were sampled for GEM by a single Tekran 2537B, located inside the adjacent mobile trailer and connected by Teflon® tubing, over five minute intervals (two 2.5 min samples on each trap consecutively). A Tekran automated Dual Switching unit (Model 1110; Tekran Inc.; Toronto, Canada) was used to switch between the two sample inlets. We used a pump to flush the inlet that was not being sampled to avoid stagnant air in the sample lines between sampling. A data logger (CR3000; Campbell Scientific; Logan, UT, USA) was used to collect data from the PRTs. More information can be found in Supp. Info. S.4.

2.2.3 Dynamic flux chamber

Further, a dynamic flux chamber constructed of Teflon was used to quantify GEM fluxes over a surface area of 0.036 m^2. The flux chamber – provided by the laboratory of M. Gustin at the University of Nevada, Reno – had a height of 6.5 cm, 2 L of volume, and 1 cm diameter holes every 2.5 cm around the chamber circumference located 2 cm above the surface to allow unrestricted airflow at 1.2 L min^{-1} during background

measurements and 4 L min^{-1} during measurements over a source tub[20]. The chamber was positioned over an area of open soil with minimal disturbance. GEM concentrations inside and outside the chambers were measured by a second 2537B Tekran Hg analyzer connected by 25 m of Teflon tubing. Switching between chamber inlet and outlet air was controlled with a Tekran Model 1115 multi-port switching unit. More information can be found in Supp. Info. S.4.

2.3. EC flux calculations

We calculated half-hour average fluxes for GEM as well as sensible and latent heat based on the covariance between turbulent fluctuations of the vertical wind speed and the scalar mixing ratios using Reynolds (block) averaging[27, 37, 38, 44, 45]. Negative fluxes reported here represent transport from the atmosphere toward the surface (deposition), while positive fluxes represent emission. For details on the post-processing of EC fluxes see Supp. Info. S.3. We assigned half-hour fluxes quality control (QC) flags: 1 (good), 2 (usable), and 3 (not usable). The following criteria were used to assign QC flags: (i) following the procedure outlined by Ruuskanen[36], the GEM cross-correlation with vertical wind speed (covariance of vertical wind speed and GEM concentrations with the latter shifted in time sample-by-sample) was visually assessed and given QC flag 1 when a well-defined peak in the cross-correlation was found within the searched time window (±10s); QC flag 2 was assigned when a less defined, but still detectable, peak was found; and QC flag 3 was assigned when no peak was observed; (ii) optimal wind directions for the sonic anemometer setup according to the manufacturer's specifications (QC flag 1: > 90° and < 270°; QC flag 2: > 45° and ≤ 90° plus ≥ 270°and < 315° ; QC flag 3: all other

cases); (iii) following [4645444343434342414 1]McMillen[46], QC flag 3 was assigned when the third rotation angle exceeded ±10° (QC flag 1 in all other cases); (iv and v) following Mauder et al. [47], QC flag 1 was assigned when the deviation of the stationarity test (a test of how variable the covariance is over time)[47], for the GEM flux or the integral similarity characteristics (a comparison with an accepted model of turbulence) was <30%, QC flag 2 was assigned for a deviation ≥30% and <100%, and QC flag 3 was assigned in all other cases. For each half-hour period, the overall QC flag was conservatively derived as the maximum QC flag of the five criteria above (Supl. Fig. S.3).

2.4 Footprint analysis

We estimated the EC flux source area (footprint) for each half-hour period with the Hsieh et al.[48] footprint model (Supp. Info. S.5, Fig. 1.b). The flux footprint is an estimate of the actual source area contributing to the GEM flux based on atmospheric conditions (e.g., wind direction, wind speed, stability), surface properties (e.g., roughness), and height of the measurement instruments[30, 31, 33, 48]. This was important for estimating the source area contributing to flux measurements as Hg-enriched surface sources were placed within 60 m of the tower and within an angle of 90° to 270°. The flux footprint is expressed as $X_{90\%}$ values representing the upwind distance from the tower within which 90% of the flux originated (source area). In addition, the concentration footprint for each of the two intake heights of the MBR system was estimated using a 3-D backward Lagrangian footprint model (LPDM-B) [33]. In contrast to the flux footprint, which was calculated for each available half-hourly period, the LPDM-B model was run with typical atmospheric conditions during the entire measurement campaign (i.e., mixing-layer

heights of 3500 and 5000 m, Monin-Obukhov lengths of -5 and -15 m, and convective velocity scales of 2 and 3 m s^{-1}, respectively). The roughness length was set to 0.01 m for bare soil in the LPDM-B model, which corresponds to the average value calculated from the logarithmic wind law under near-neutral atmospheric conditions when winds originated from the 90-270° sector.

3. Results and discussion

3.1. High-frequency signal analysis

We thoroughly checked collected GEM concentrations for data quality before calculation of EC fluxes, including Allan variance plots (Supp. Fig. S.4), (co-)spectral (Fig. 2) and cross-correlation analysis (Fig. 3); these served to validate GEM concentration measurements and supported processing data prior to calculating fluxes (as detailed below). We used Allan variance plots to assess the stability of GEM concentration measurements through time. An example, shown in Supp. Fig. S.4, demonstrates that the variance of high-resolution GEM measurements (red line) during stable background conditions decreased with a slope inversely proportional to the integration time until approximately 50 s. The Allan variance started to increase after an integration time of approximately 200 s with a slope proportional to the integration time. The latter is an indication of linear drift of the CRDS system causing an increase in the GEM variance at longer integration times[49]. In order to account for this instrument drift, which would result in an overestimation of GEM flux calculations, we corrected CRDS GEM signals using GEM concentrations measured downstream of the CRDS with a slower-time response (2.5 min) Model 2537B Tekran Hg analyzer. To this end, we

248 calibrated CRDS GEM data every 2.5 min with concentrations measured by the Model
249 2537B. As shown in Supp. Fig. S.4, this procedure (blue line) effectively removed low-
250 frequency drifts, causing the variance to decrease with a slope inversely proportional to
251 the integration time through 1000 s.

252 We used spectral and co-spectral analyses to compare the quality of the CRDS GEM
253 signals with the temperature data as measured by the sonic anemometer in the frequency
254 domain[50]. Power spectra and co-spectra, typical for QC 1, are shown in Fig. 2. This
255 comparison between temperature and GEM power spectra showed that the GEM signal
256 started to be dominated by noise above frequencies of 0.45 Hz, causing it to deviate from
257 the expected $f^{-5/3}$ (where f is frequency) decay in the inertial sub-range (solid line Fig. 2a)
258 and the temperature spectrum measured with the sonic anemometer[51]. The co-spectra of
259 vertical wind speed with temperature and GEM, respectively, generally agreed in the
260 lower frequency range and up to around 0.2 Hz, indicating that the removal of the linear
261 drift in the GEM signals was successful (Fig. 2b). At frequencies around 0.2 Hz, the
262 GEM co-spectrum started to roll off, which is indicative of low-pass filtering by the
263 measurement system (in particular attenuation of concentration fluctuations down the
264 sampling tube)[52]. The dashed line in Fig. 2b represents the co-spectral reference model
265 convolved with a series of transfer functions which account for all sources of low-pass
266 filtering (Supp. Inf. S.3). Our approach of correcting for low-pass filtering was able to
267 reproduce (and thus allowed correcting for) this flux loss [51, 52]. At frequencies >0.45 Hz
268 (which corresponds to ca. 12% of total flux), the noise observed in the GEM spectra (Fig.
269 2a) compensated for the low-pass filtering and even caused an increase in co-spectral
270 density, while the temperature co-spectrum further decreased in the inertial sub-range as

271 expected[51] (Fig. 2b). In order to remove the noise in the high-frequency part of the GEM
272 co-spectrum, we used a low-pass Finite Impulse Response (FIR) filter[51] with a time
273 constant of 2 s to filter out any unwanted contributions at frequencies >0.45Hz. The
274 missing high-frequency (>0.2 Hz) flux contribution due to low-pass filtering by the
275 measurement system and the low-pass FIR filter (>0.45 Hz) was then back-corrected
276 based on the reference model co-spectrum of Kaimal and Finnigan[51]. The resulting
277 average frequency response correction factor was 1.89 (range 1.29–2.58).

278 **Figure 2**

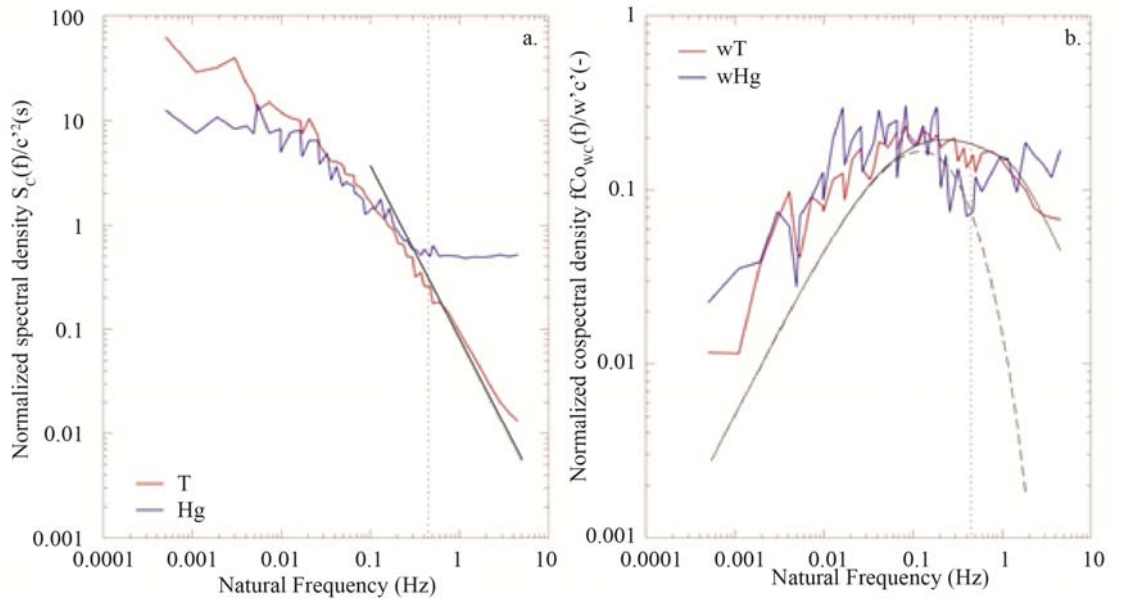

279

280

281 We used a cross-correlation analysis to identify whether a covariance existed between
282 vertical wind speed and GEM concentration for each half hour sampled. Following
283 Ruuskanen et al.[36], a well-defined peak in the cross-correlation analysis (Fig. 3) indicated

284 a significant correlation between vertical wind speed and GEM concentration from which
285 a flux was calculated. Figure 3 demonstrates examples of a well-defined peak in the
286 cross-correlation between GEM and vertical wind speed (assigned QC 1) as well as a
287 lower quality peak (assigned QC 2), which was associated with higher uncertainty. A
288 lack of cross-correlation (assigned QC 3) indicated fluxes close to zero, which may be
289 because no fluxes existed or because fluxes were below the detection limit of the system.
290 The time lag shown in the cross-correlation analysis, as indicated by the shift in the peak
291 covariance, at roughly 3.3 s represents the time for sample air to travel from the sample
292 inlet on the EC tower (where vertical wind speed was measured) to the CRDS system
293 inside the measurement trailer (where GEM was measured). This time lag, which was
294 consistent throughout the measurements, was used to properly align all vertical wind
295 speed and GEM concentration data for covariance calculations.

296 **Figure 3**

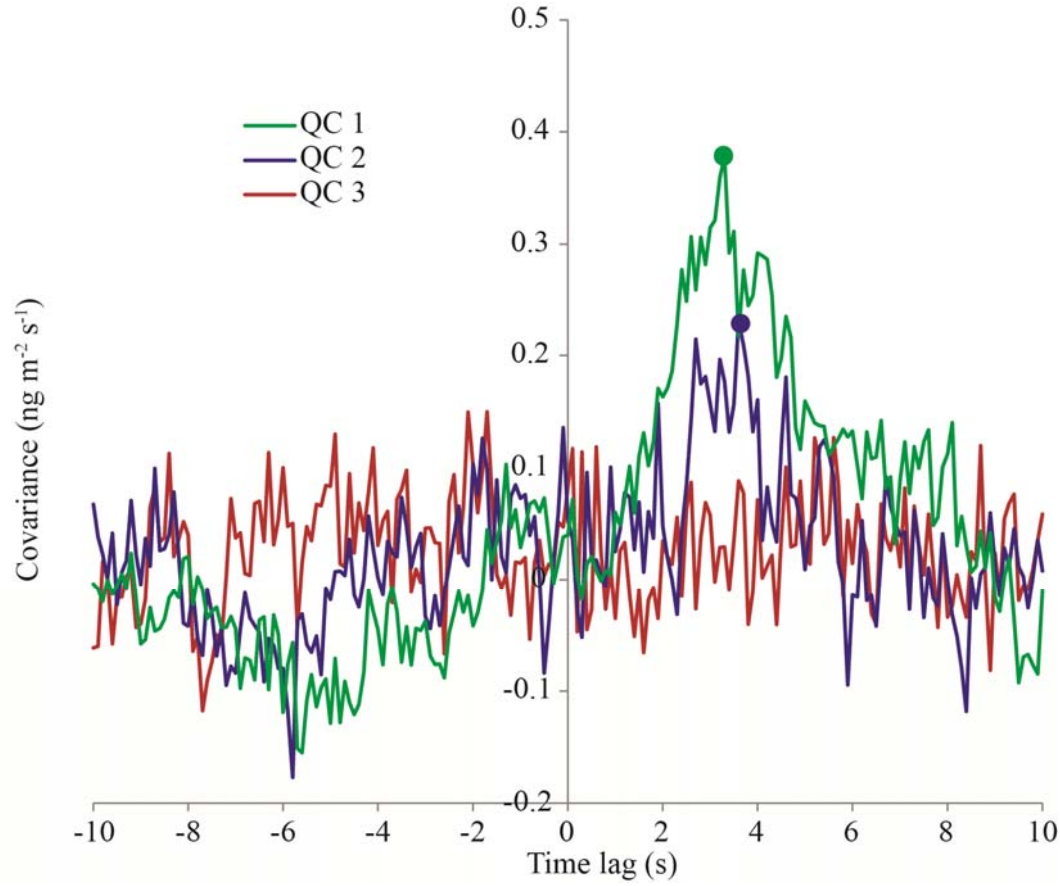

297

298 Of a total of 85 half-hour measurements, 17%, 21%, and 62% fell into the overall QC
299 classes 1, 2, and 3, respectively (Supp. Fig. S.3), and 57% of the data in QC 3 was due to
300 lack of a clear cross-correlation. During sampling under background conditions, all
301 available half-hour fluxes failed to meet the cross-correlation criterion (i.e., fluxes close
302 to zero and/or below detection limit). During deployment of the Hg-enriched soils, 43%
303 of the data failed to meet the cross-correlation criterion, which usually was associated
304 with air masses originating from outside the Hg-enriched soil area. Overall, the wind
305 direction, stationarity, integral turbulence, and third rotation angle criteria were not
306 fulfilled in 7, 11, 0, and 1% of all cases.

Several methods were used to evaluate the detection limit of the EC flux system. The smallest, absolute detected GEM flux with a clear cross-correlation was 32 ng m^{-2} h^{-1} (QC 2), Using the method described in Pihlatie et al. (2005)[53], which requires the standard deviation of vertical wind speed and the noise level of the instrument (30 min standard deviation during background measurements), we calculated a flux detection limit of 2-60 ng m^{-2} h^{-1}. Standard deviation of vertical wind speed varied between 0.20-0.45 m s^{-1}. The standard deviation of GEM during background measurements varied between 0.0022-0.0050 μg m^{-3}. This flux detection limit is similar to the smallest absolute detected GEM flux of 32 ng m^{-2} h^{-1}. However, using the power spectra of the background noise (before Hg-enriched soil boxes were in place) and an estimate of the vertical wind power spectra as described in Pattey et al. (2006)[54], we calculated a flux detection limit of 82-195 ng m^{-2} h^{-1} for the range of observed wind speeds of 0.3-4 m s^{-1}. This technique gives a higher flux detection limit. Following Wienhold et al. (2005) a signal-to-noise (S/N) ratio analysis was performed. For the 85 half-hour periods of calculated fluxes, 33% exceed a S/N of 3. In QC 1 S/N varied from 4.1 to 9.5 (100% S/N > 3), QC 2 S/N varied from 2.6 to 9.2 (95% S/N > 3) and QC 3 S/N varied from 1.8 to 23.4 (72% S/N > 3). This indicates that for QC 1 and 2 S/N ratios were generally above 3. Although some fluxes with acceptable S/N ratios were rejected in QC 3, the use of other quality criteria in this case assures us that these fluxes are not useable (Supp. Fig. S.3 and S.5).

3.2. EC GEM fluxes

Mean background afternoon (12:00–18:00) ambient air GEM concentrations measured with a Model 2537B analyzer were 1.42 ng m^{-3} with a range of 1.20 to 2.23 ng m^{-3} prior to the Hg-enriched soil being deployed and 1.53 ng m^{-3} with a range of 1.06 to 2.85 ng m^{-3} after removal. During the three days of background flux measurements, GEM fluxes calculated with the EC method (Table 1; Fig. 1b, left panel) all failed the cross-correlation criteria (QC 3). As a result, all of these fluxes can be considered below the detection limit of the system.

When the Hg-enriched soil was deployed (Sept. 19 to 28), mean ambient air GEM concentrations increased to 3.75 ng m^{-3} with a range of 0.68 to 21.40 ng m^{-3}. The LPMD-B footprint model showed that during typical afternoon conditions, the source area ($X_{90\%}$) for 80% of the half-hour EC GEM fluxes originated within 14 to 18 m of the measurement tower, well within the area where Hg-enriched soil sources were deployed (extending 60 m). As expected, the highest fluxes (1000–3200 ng m^{-2} h^{-1}) commonly were observed during periods when $X_{90\%}$ fell within the Hg-enriched area. As can be seen in Figure 1b, large fluxes (>1000 ng m^{-2} h^{-1}) also were observed on three occasions where $X_{90\%}$ values were beyond, but closely adjacent to, the Hg-enriched soil sources (discussed below). Lower fluxes, below 1000 ng m^{-2} h^{-1} and often below 500 ng m^{-2} h^{-1}, occurred mainly when fluxes originated from wind directions outside the Hg-enriched soil sources and during background measurements. GEM fluxes derived with all methods increased (Table 1), and EC GEM fluxes were more consistently classified as QC 1 and QC 2 (Fig. 1b, right panel; Supp. Fig. S.3). Figure 1b shows flux magnitudes and the source area of GEM fluxes expressed as $X_{90\%}$ for all 85 half-hour GEM EC measurements.

352 **Table 1.** Comparison of fluxes over background and Hg-enriched soils derived using all
353 three techniques.

Background measurements	Mean	Min	Max	StdError	n	% no cross-correlation
GEM (ng m^{-3})*	1.48	1.06	2.85	0.01	448	
EC (ng m^{-2} h^{-1}) **	<MDL***	<MDL	<MDL	<MDL	<MDL	100
MBR (ng m^{-2} h^{-1}) **	-76	-265	50	17	20	-
DFC (ng m^{-2} h^{-1})	0.01	-8.9	6.8	0.09	277	-
Hg-enriched area measurements						
GEM (ng m^{-3})*	3.75	0.68	21.40	0.09	743	
EC QC 1 (ng m^{-2} h^{-1})	1105	71	2339	180	14	0
EC QC 1&2 (ng m^{-2} h^{-1})	849	-304	2339	111	32	0
MBR QC 1 (ng m^{-2} h^{-1})	1712	-795	3934	367	14	-
MBR QC 1&2 (ng m^{-2} h^{-1})	1309	-1026	3934	217	32	-
DFC (ng m^{-2} h^{-1})	1105	23	3848	68	150	-

354 *atmospheric concentrations measured by Tekran 2537B
355 **all background EC fluxes were QC 3 and had no cross-correlation, MBR fluxes were below the
356 minimum resolvable gradient (MRG)
357 ***MDL = 32 ng m^{-2} h^{-1}
358

359 In general, GEM fluxes measured with the EC method when the Hg-enriched soil
360 boxes were deployed had a wide range of values (QC 1&2 standard deviation ± 626.4;
361 Supp. Fig S.6). Fluxes previously reported from naturally Hg-enriched soils [23], fluxes
362 measured in large ecologically controlled lysimeter laboratories (EcoCELLs) over Hg
363 amended soils [55], and fluxes calculated from DFC measurements using Hg-enriched
364 substrates [56-58] showed a range that spanned five orders of magnitude in comparison to
365 our measurements. We believe the measurement set-up contributed most of this
366 variability (Table 1); and, in particular, the differences between GEM fluxes over the Hg-
367 enriched soil and background soil area. The Hg-enriched soil boxes were limited to a

semi-circle from due east through south to due west (Fig. 1a), and it was likely that variability in EC GEM fluxes was induced by flux source areas switching between background and Hg-enriched areas (e.g., an "edge effect", during any half-hourly averaging period). Another possibility is that environmental conditions caused some of the variability. This is unlikely since measurements were taken during relatively unstable conditions in afternoon hours, with no major precipitation events occurring.

To highlight the edge effect, Fig. 4 shows three days of EC and MBR flux measurements that were impacted differently by the Hg-enriched soil area due to changes in dominant wind directions. On September 19, all measurements corresponded to average wind directions from the Hg-enriched area (between 90° and 270°). Fluxes were highest when the wind direction was centered within the Hg-enriched soil area and as winds moved towards the edge and out of this area, measured fluxes decreased. All measurement points on September 19 were characterized as QC 1 and 2. The edge effect also was obvious on September 28 when dominant winds first originated from the Hg-enriched soil area (first three measurements), but fluxes dropped significantly after the flux source area moved into the background soil area. While the initial three measurement points were characterized as QC 1 and 2, the last four points were characterized as QC 3 due to a lack of a cross-correlation and acceptable wind direction, and were consistent with lower GEM fluxes expected over the background soil area. Finally, on September 24, all measurements were taken when the flux source area was located outside of the Hg-enriched soil area, and fluxes, although relatively small, should be considered with caution during this period since five of the seven points were characterized as QC 3 data.

391 The examples on September 19, 24, and 28 show sensitivity of the EC measurements to
392 wind directions shifting over the Hg-enriched soil area. It is further possible that
393 additional flux variability was due to the deployment of discrete Hg sources; these
394 sources were placed in boxes to avoid contamination of the site with 10 m in between,
395 and the emissions from these tubs may not have been thoroughly mixed in the
396 atmosphere prior to measurements at the EC tower, inducing additional variability both in
397 concentrations and calculated fluxes.

398 **Figure 4**

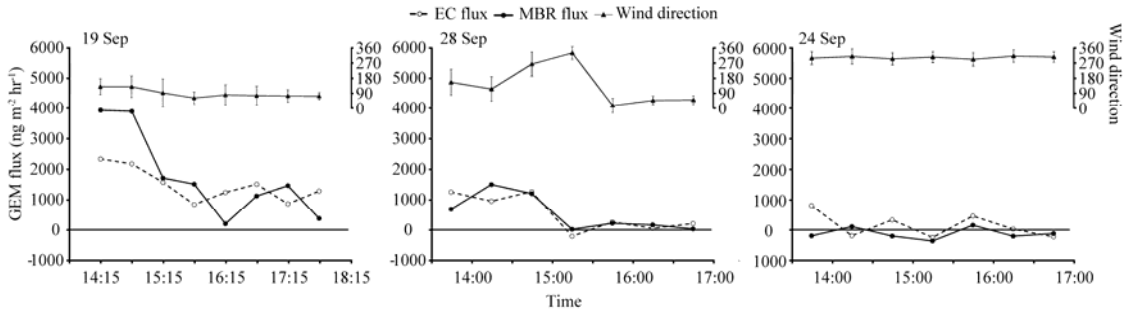

399

400 *3.3 Comparison of GEM flux measurement methods*

401 We compared EC fluxes with measurements from two other flux measurement
402 methods, the MBR method and a DFC. Over background soils, mean GEM fluxes
403 measured with the DFC (Table 1) were within the range of GEM fluxes measured with
404 DFCs in other background areas (ranging from -1 to 45 ng m^{-2} hr^{-1})[24, 59, 60] and over
405 background soils in Nevada (averaging 1.0 to 2.0 ng m^{-3} h^{-1}; with ranges of -3.7 to 9.3 ng
406 m^{-2} h^{-1})[61-63]. The range of measured EC GEM fluxes was substantially higher than those
407 measured with the DFC and actually showed an average depositional flux across all
408 background measurements of -43 ng m^{-2} hr^{-1}. We considered these measured EC fluxes
409 over background soils unreasonable (both regarding variability and magnitude) as

410 compared to background soil fluxes reported by other studies and our own background
411 GEM fluxes measured by the DFC method. This is supported by all of the EC fluxes
412 falling into the QC 3 category with no detectible cross-correlation between GEM and
413 wind speed.

414 The issue with many GEM fluxes falling below the detection limit was not unique to
415 the EC method but was also apparent in fluxes measured with the MBR method
416 (averaging -76 ng m^{-2} hr^{-1}). Resolving very small vertical gradients between two
417 measurement heights is challenging over non-contaminated background sites, which was
418 further exacerbated by a short separation (0.51 m) between measurement inlets compared
419 to more commonly used gradients of 2 to 4 m. In this study, the small vertical separation
420 was necessary to restrict flux footprints to the Hg-enriched soil area (60 m upwind).
421 Other GEM fluxes measured with micrometeorological methods over background
422 ecosystems fell in the range of -68 to 34 ng m^{-2} hr^{-1}[21, 28, 62, 64] and often showed high
423 variability as well. Calculated minimum resolvable gradients (MRG) between the two
424 GEM inlets in MBR setups are in the range of 0.01 to 0.05 ng m^{-3} in several studies[21, 31,
425 64]. During our background measurements, MBR gradients averaged 0.04 ng m^{-3} with a
426 range of -0.04 to 0.16 ng m^{-3}, and 50% of the data was below an absolute value of 0.05
427 ng m^{-3} which was the smallest detectable gradient in a previous study [21].

428 Unlike under background conditions, GEM fluxes measured with the EC, MBR, and
429 DFC methods over the Hg-enriched soil area were in similar ranges, generally in the
430 same direction (emission or deposition), and showed similar average fluxes and temporal
431 patterns (Table 1). Fluxes measured with DFCs have been reported to be lower than those
432 measured with micrometeorological methods[22, 23], which was not the case for our

433 measurements. Figure 4 shows a flux comparison between EC and MBR measurements
434 for the three days that were presented above to discuss the effects of wind direction. The
435 patterns show that EC and MBR measurements compared well during these days,
436 showing similar temporal patterns and magnitudes of fluxes. This may indicate that
437 conditions that were favorable or unfavorable for the EC measurements, based on
438 spectral analysis, are similarly favorable or unfavorable for the MBR method. For
439 September 19, when all EC measurements fell into QC 1 and 2, the coefficient of
440 determination, r^2, of a significant linear regression between EC and MBR method was
441 0.62 and showed a slope of 2, although the r^2 and slope decreased to 0.53 and 1.3,
442 respectively, when the regression was forced through the zero offset. The linear
443 regression for September 28 had an r^2 of 0.7 and a slope of 0.82 which decreased to 0.68
444 and 0.9, respectively, when forced through the zero offset. No significant linear
445 regression between EC and MBR measurements, however, was found on September 24
446 when most of the data fell into QC 3.

447 GEM fluxes measured with the MBR method showed an even higher range of values
448 and greater variability than to the EC measurements (Table 1). One possible reason for
449 this includes potentially different concentration footprints for the MBR method, which
450 has two different inlets at heights of 0.58 m and 1.09 m, respectively, compared to the EC
451 method (single inlet at 0.75 m). However, concentration footprint distances amounted to
452 8–10 m and 18–22 m for the two different gradient intake heights for typical afternoon
453 conditions and hence were clearly located within the 60 m source area. Therefore, the
454 different inlet heights of the EC and MBR methods cannot explain the observed
455 differences between the two methods or the more variable MBR flux data.

456

457 Conclusions

458 Wesuccessfully demonstrated applicability of the EC method for GEM flux
459 measurements by detection of well-defined covariance between high-resolution
460 measurements of vertical wind speed and GEM concentrations. Such field measurements
461 were challenging since they required deployment of a complex and highly sensitive
462 optical CRDS system in the field with significant demands for protecting the system from
463 vibrations, temperature and power fluctuations, and dust. Calculated GEM fluxes were in
464 the range of other flux methods under Hg enrichment, and showed high sensitivity to the
465 presence of Hg-enriched soil with changing fluxes as wind direction changed over the
466 source area. There was good comparison between the three flux measurement techniques
467 when conditions were favorable for flux measurements over the Hg-enriched source area
468 (QC 1 & 2). These measurements, to our knowledge, represent the first-ever EC
469 measurements performed to quantify GEM surface exchange. It proved to be
470 straightforward to detect EC fluxes over the Hg-enriched soil area, but detection was not
471 feasible over natural background areas in the existing setup with the current CRDS
472 sensitivity. The smallest, absolute, detectable flux with our system was 32 ng m^{-2} h^{-1}, and
473 we conclude that this flux was a conservative estimate of the system's flux detection
474 limit. Various system improvements could be implemented to increase flux detection
475 limits and time coverage of measurements, including increasing the sensitivity of the
476 CRDS GEM detection limit, (e.g., by increasing cavity path lengths to improve
477 sensitivity), new cavity designs targeted at reducing flow interferences for EC
478 measurements (reduce noise evident in the GEM spectra and co-spectra and eliminate

reliance on a slow-response instrument for data correction), and advancements to the system to make it more robust for longer-term field deployments.

Figure Caption

Figure 1: a.) Site schematic; blue area represents the area with deployed Hg-enriched soil boxes (represented by square dots), and dashed lines indicate the 10 m^2 spacing around each individual source tub. b.) Flux measurement over background soils (left panel) and over Hg-enriched areas (right panel) and associated flux footprints. Symbol colors represent flux magnitude, and location show X_{90}% values, which represent upwind distance from tower within which 90% of the flux originated, based on footprint analysis (note micrometeorological tower located in the center). Solid symbols indicate QC 1 data, open symbols indicate QC 2 data, crossed out symbols indicate QC 3 data. The blue area on the right panel indicates deployed Hg-enriched soil boxes. c.) Wind rose for the measurement period.

Figure 2: a.) Power spectra of sonic temperature (T) and GEM (Hg) (left panel) and corresponding co-spectra with vertical wind speed (right panel). Lines represent ensemble averages from 19 September 2012 14-17:00 local time (mean wind speed 1.8 m s^{-1} and unstable conditions). The dotted vertical line indicates the onset of noise (0.45 Hz). The solid line in the left panel shows the expected $f^{5/3}$ slope in the inertial subrange. The solid and dashed lines in the right panel refer to the cospectral reference model by Kaimal and Finnigan (1994) and the cospectral reference model attenuated by a series of

transfer functions that represent the effects of low-pass filtering on the GEM time series, respectively.

Figure 3: Cross-correlation analysis of vertical wind speed with GEM density. The red, blue and green lines refer to cases of a well-defined peak in the cross-correlation (QC flag 1; 19.09.2012 14:00-14:30, average horizontal wind speed = 2.3 m s^{-1}, Monin-Obukhov stability parameter = -0.15), a less well-defined peak (QC flag 2; 19.09.2012 17:30-18:00, average horizontal wind speed = 2.9 m s^{-1}, Monin-Obukhov stability parameter = -0.04) and no detectable peak (QC flag 3; 20.09.2012 16:30-17:00, average horizontal wind speed = 2.9 m s^{-1}, Monin-Obukhov stability parameter = -0.13).

Figure 4: GEM fluxes (ng m^{-2} h^{-1}) as measured by the CRDS system (filled dots) and the MBR method (open dots) during three specific days with different wind directions and therefore different impact of the deployed Hg-enriched sources. Shaded areas represent the angles corresponding to the deployed Hg-enriched substrate upwind of the measurement towers; wind directions are average wind directions during the respective 30 min. measurement periods and show the degree to which dominant wind directions corresponded to the upwind Hg-enriched source area. Wind direction error bars are standard deviation of the wind direction.

Supporting Information

The supporting information includes further information of the field site and meteorology, data processing, auxiliary instruments, flux footprints and flux comparisons. This material is available free of charge via the Internet at http://pubs.acs.org.

Corresponding author

*Corresponding author: Desert Research Institute, 2215 Raggio Parkway, Reno, NV 89512. Phone: (775) 674-7008 Fax: (775) 674-7016 Email: daniel.obrist@dri.edu

Present address

†University of Nevada, Reno, 1664 N. Virginia st. Reno, NV USA

Author Contributions

The manuscript was written through contributions of all authors. All authors have given approval to the final version of the manuscript.

Acknowledgements

We would like to thank Rick Purcell for technical assistance and engineering, Brad Lyles for his help with the eddy covariance tower set up, Roger Kreidberg for editorial assistance, Mike Crumb for technical laser assistance, Mae Gustin for use of the DFC and Tekran Automated Dual Switching units, and the facilities crew at the Desert Research Institute for help with mobile trailer setup. We also would like to thank Mitch Goldfin and his parents for allowing us access to their land. This study was supported by a U.S.

542 National Science Foundation Major Instrumentation (NSF MRI) grant (NSF AGS Award
543 #0923485).

544

545

References

1. Rothenberg, S. E.; Mckee, L.; Gilbreath, A.; Yee, D.; Connor, M.; Fu, X. W., Evidence for short-range transport of atmospheric mercury to a rural, inland site. *Atmos Environ* **2010,** *44*, (10), 1263-1273.
2. Fitzgerald, W. F.; Engstrom, D. R.; Mason, R. P.; Nater, E. A., The Case for Atmospheric Mercury Contamination in Remote Areas. *Environmental Science & Technology* **1998,** *32*, (1), 1-7.
3. Obrist, D.; Hallar, A. G.; McCubbin, I.; Stephens, B. B.; Rahn, T., Atmospheric mercury concentrations at Storm Peak Laboratory in the Rocky Mountains: Evidence for long-range transport from Asia, boundary layer contributions, and plant mercury uptake. *Atmos Environ* **2008,** *42*, (33), 7579-7589.
4. Lindberg, S.; Bullock, R.; Ebinghaus, R.; Engstrom, D.; Xinbin, F.; Fitzgerald, W.; Pirrone, N.; Prestbo, E.; Seigneur, C., A Synthesis of Progress and Uncertainties in Attributing the Sources of Mercury in Deposition. *AMBIO - A Journal of the Human Environment* **2007,** *36*, (1), 19-32.
5. Zhang, L.; Wright, L. P.; Blanchard, P., A review of current knowledge concerning dry deposition of atmospheric mercury. *Atmos Environ* **2009,** *43*, (37), 5853-5864.
6. Ericksen, J. A.; Gustin, M. S.; Lindberg, S. E.; Olund, S. D.; Krabbenhoft, D. P., Assessing the potential for re-emission of mercury deposited in precipitation from arid soils using a stable isotope. *Environmental Science & Technology* **2005,** *39*, (20), 8001-8007.
7. Lalonde, J. D.; Poulain, A. J.; Amyot, M., The role of mercury redox reactions in snow on snow-to-air mercury transfer. *Environmental Science and Technology* **2002,** *36*, (2), 174 -178.
8. Carpi, A.; Lindberg, S. E., Sunlight-mediated emission of elemental mercury from soil amended with municipal sewage sludge. *Environ. Sci. Technol.* **1997,** *31*, (7), 2085-2091.
9. Amyot, M.; Mierle, G.; Lean, D.; McQueen, D. J., Effect of solar radiation on the formation of dissolved gaseous mercury in temperate lakes. *Geochimica Et Cosmochimica Acta* **1997,** *61*, (5), 975-987.
10. Amyot, M.; Mierle, G.; Lean, D. R. S.; McQueen, D. J., Sunlight-induced formation of Dissolved Gaseous Mercury in Lake waters. *Environmental Science and Technology* **1994,** *28*, 2366-2371.
11. Alberts, J. J.; Schindler, J. E.; Miller, R. W.; Nutter Jr., D. E., Elemental Mercury Evolution Mediated by Humic Acid. *Science* **1974,** *184*, (4139), 895-897.
12. Allard, B.; Arsenie, I., Abiotic Reduction of Mercury by Humic Substances in Aquatic System - an Important Process for the Mercury Cycle. *Water Air and Soil Pollution* **1991,** *56*, 457-464.
13. Mason, R. P.; Morel, F. M. M.; Hemond, H. F., The Role of Microorganisms in Elemental Mercury Formation in Natural Waters. *Water Air and Soil Pollution* **1995,** *80*, (1-4), 775-787.
14. Barkay, T.; Liebert, C.; Gillman, M., Environmental significance of the potential for mer(Tn21)-mediated reduction of Hg2+ to Hg0 in natural-waters. *Applied and Environmental Microbiology* **1989,** *55*, (5), 1196-1202.
15. Obrist, D.; Faïn, X.; Berger, C., Gaseous elemental mercury emissions and CO_2 respiration rates in terrestrial soils under controlled aerobic and anaerobic conditions. *The Science of The Total Environment* **2010,** *408*, 1691-1700.
16. Corbitt, E. S.; Jacob, D. J.; Holmes, C. D.; Streets, D. G.; Sunderland, E. M., Global Source–Receptor Relationships for Mercury Deposition Under Present-Day and 2050 Emissions Scenarios. *Environmental Science & Technology* **2011,** *45*, (24), 10477-10484.

592 17. Axelrad, D. A.; Bellinger, D. C.; Ryan, L. M.; Woodruff, T. J., Dose-Response Relationship
593 of Prenatal Mercury Exposure and IQ: An Integrative Analysis of Epidemiologic Data.
594 *Environmental Health Perspectives* **2007,** *115*, (4), 609-615.
595 18. Booth, S.; Zeller, D., Mercury, Food Webs, and Marine Mammals: Implications of Diet
596 and Climate Change for Human Health. *Environmental Health Perspectives* **2005,** *113*, (5), 521-
597 526.
598 19. Clarkson, T. W.; Magos, L., The Toxicology of Mercury and Its Chemical Compounds.
599 *Critical Reviews in Toxicology* **2006,** *36*, (8), 609-662.
600 20. Eckley, C. S.; Gustin, M.; Lin, C. J.; Li, X.; Miller, M. B., The influence of dynamic chamber
601 design and operating parameters on calculated surface-to-air mercury fluxes. *Atmos Environ*
602 **2010,** *44*, (2), 194-203.
603 21. Fritsche, J.; Obrist, D.; Zeeman, M. J.; Conen, F.; Eugster, W.; Alewell, C., Elemental
604 mercury fluxes over a sub-alpine grassland determined with two micrometeorological methods.
605 *Atmos Environ* **2008,** *42*, (13), 2922-2933.
606 22. Gustin, M. S.; Rasmussen, P.; Edwards, G.; Schroeder, W.; Kemp, J., Application of a
607 laboratory gas exchange chamber for assessment of in situ mercury emissions. *J. Geophys. Res.*
608 **1999,** *104*, (D17), 21873-21878.
609 23. Gustin, M. S.; Lindberg, S.; Marsik, F.; Casimir, A.; Ebinghaus, R.; Edwards, G.; Hubble-
610 Fitzgerald, C.; Kemp, R.; Kock, H.; Leonard, T.; London, J.; Majewski, M.; Montecinos, C.; Owens,
611 J.; Pilote, M.; Poissant, L.; Rasmussen, P.; Schaedlich, F.; Schneeberger, D.; Schroeder, W.;
612 Sommar, J.; Turner, R.; Vette, A.; Wallschlaeger, D.; Xiao, Z.; Zhang, H., Nevada STORMS project:
613 Measurement of mercury emissions from naturally enriched surfaces. *J. Geophys. Res.* **1999,**
614 *104*, (D17), 21831-21844.
615 24. Carpi, A.; Lindberg, S. E., Application of a teflon™ dynamic flux chamber for quantifying
616 soil mercury flux: Tests and results over background soil. *Atmos Environ* **1998,** *32*, (5), 873-882.
617 25. Bash, J. O.; Miller, D. R., Growing season total gaseous mercury (TGM) flux
618 measurements over an Acer rubrum L. stand. *Atmos Environ* **2009,** *43*, (37), 5953-5961.
619 26. Lindberg, S. E.; Kim, K.-H.; Meyers, T. P.; Owens, J. G., Micrometeorological Gradient
620 Approach for Quantifying Air/Surface Exchange of Mercury Vapor: Tests Over Contaminated
621 Soils. *Environmental Science & Technology* **1995,** *29*, (1), 126-135.
622 27. Arya, S. P., *Introduction to Micrometeorology*. Academic Press: San Diego, 2001.
623 28. Kim, K.-H.; Lindberg, S. E.; Meyers, T. P., Micrometeorological measurements of mercury
624 vapor fluxes over background forest soils in eastern Tennessee. *Atmos Environ* **1995,** *29*, (2),
625 267-282.
626 29. Meyers, T. P.; Hall, M. E.; Lindberg, S. E.; Kim, K., Use of the modified bowen-ratio
627 technique to measure fluxes of trace gases. *Atmos Environ* **1996,** *30*, (19), 3321-3329.
628 30. Converse, A. D.; Riscassi, A. L.; Scanlon, T. M., Seasonal variability in gaseous mercury
629 fluxes measured in a high-elevation meadow. *Atmos Environ* **2010,** *44*, (18), 2176-2185.
630 31. Edwards, G. C.; Rasmussen, P. E.; Schroeder, W. H.; Wallace, D. M.; Halfpenny-Mitchell,
631 L.; Dias, G. M.; Kemp, R. J.; Ausma, S., Development and evaluation of a sampling system to
632 determine gaseous Mercury fluxes using an aerodynamic micrometeorological gradient method.
633 *J Geophys Res-Atmos* **2005,** *110*, (D10), ---.
634 32. Zuo, J.; Huang, J.; Wang, J.; Zhang, W.; Bi, J.; Wang, G.; Li, W.; Fu, P., Surface turbulent
635 flux measurements over the Loess Plateau for a semi-arid climate change study. *Advances in*
636 *Atmospheric Sciences* **2009,** *26*, (4), 679-691.

33. Kljun, N.; Rotach, M. W.; Schmid, H. P., A three-dimensional backward lagrangian footprint model for a wide range of boundary-layer stratifications. *Boundary-Layer Meteorology* **2002,** *103*, (2), 205-226.
34. Cobos, D. R.; Baker, J. M.; Nater, E. A., Conditional sampling for measuring mercury vapor fluxes. *Atmos Environ* **2002,** *36*, (27), 4309-4321.
35. Bash, J. O.; Miller, D. R., A Relaxed Eddy Accumulation System for Measuring Surface Fluxes of Total Gaseous Mercury. *Journal of Atmospheric & Oceanic Technology* **2008,** *25*, (2), 244-257.
36. Ruuskanen, T. M.; Müller, M.; Schnitzhofer, R.; Karl, T.; Graus, M.; Bamberger, I.; Hörtnagl, L.; Brilli, F.; Wohlfahrt, G.; Hansel, A., Eddy covariance VOC emission and deposition fluxes above grassland using PTR-TOF. *Atmos. Chem. Phys.* **2011,** *11*, (2), 611-625.
37. Aubinet, M.; Grelle, A.; Ibrom, A.; Rannik, Ü.; Moncrieff, J.; Foken, T.; Kowalski, A. S.; Martin, P. H.; Berbigier, P.; Bernhofer, C.; Clement, R.; Elbers, J.; Granier, A.; Grünwald, T.; Morgenstern, K.; Pilegaard, K.; Rebmann, C.; Snijders, W.; Valentini, R.; Vesala, T., Estimates of the Annual Net Carbon and Water Exchange of Forests: The EUROFLUX Methodology. In *Advances in Ecological Research*, Raffaelli, A. H. F. a. D. G., Ed. Academic Press: 1999; Vol. Volume 30, pp 113-175.
38. Baldocchi, D. D.; Hincks, B. B.; Meyers, T. P., Measuring Biosphere-Atmosphere Exchanges of Biologically Related Gases with Micrometeorological Methods. *Ecology* **1988,** *69*, (5), 1331-1340.
39. Baldocchi, D.; Falge, E.; Gu, L.; Olson, R.; Hollinger, D.; Running, S.; Anthoni, P.; Bernhofer, C.; Davis, K.; Evans, R.; Fuentes, J.; Goldstein, A.; Katul, G.; Law, B.; Lee, X.; Malhi, Y.; Meyers, T.; Munger, W.; Oechel, W.; Paw, K. T.; Pilegaard, K.; Schmid, H. P.; Valentini, R.; Verma, S.; Vesala, T.; Wilson, K.; Wofsy, S., FLUXNET: A New Tool to Study the Temporal and Spatial Variability of Ecosystem–Scale Carbon Dioxide, Water Vapor, and Energy Flux Densities. *Bulletin of the American Meteorological Society* **2001,** *82*, (11), 2415-2434.
40. Baldocchi, D. D., Assessing the eddy covariance technique for evaluating carbon dioxide exchange rates of ecosystems: past, present and future. *Global Change Biology* **2003,** *9*, (4), 479-492.
41. Aubinet, M.; Chermanne, B.; Vandenhaute, M.; Longdoz, B.; Yernaux, M.; Laitat, E., Long term carbon dioxide exchange above a mixed forest in the Belgian Ardennes. *Agricultural and Forest Meteorology* **2001,** *108*, (4), 293-315.
42. Pierce, A.; Obrist, D.; Moosmüller, H.; Faïn, X.; Moore, C., Cavity ring-down spectroscopy sensor development for high-time-resolution measurements of gaseous elemental mercury in ambient air. *Atmospheric Measurement Techniques* **2013,** *6*, (6), 1477-1489.
43. Faïn, X.; Moosmüller, H.; Obrist, D., Toward real-time measurement of atmospheric mercury concentrations using cavity ring-down spectroscopy. *Atmospheric Chemistry & Physics* **2010,** *10*, (6), 2879-2892.
44. Wohlfahrt, G.; Hammerle, A.; Haslwanter, A.; Bahn, M.; Tappeiner, U.; Cernusca, A., Seasonal and inter-annual variability of the net ecosystem CO2 exchange of a temperate mountain grassland: Effects of weather and management. *J. Geophys. Res.* **2008,** *113*, (D8), D08110.
45. Haslwanter, A.; Hammerle, A.; Wohlfahrt, G., Open-path vs. closed-path eddy covariance measurements of the net ecosystem carbon dioxide and water vapour exchange: A long-term perspective. *Agricultural and Forest Meteorology* **2009,** *149*, (2), 291-302.

682 46. McMillen, R. T., An Eddy-Correlation Technique with Extended Applicability to Non-
683 Simple Terrain. *Boundary-Layer Meteorology* **1988,** *43*, (3), 231-245.
684 47. Mauder, M.; Foken, T.; Clement, R.; Elbers, J. a.; Eugster, W.; Grünwald, T.; Heusinkveld,
685 B.; Kolle, O., Quality control of CarboEurope flux data – Part 2: Inter-comparison of eddy-
686 covariance software. *Biogeosciences* **2008,** *5*, (2), 451-462.
687 48. Hsieh, C.-I.; Katul, G.; Chi, T.-w., An approximate analytical model for footprint
688 estimation of scalar fluxes in thermally stratified atmospheric flows. *Advances in Water*
689 *Resources* **2000,** *23*, (7), 765-772.
690 49. Werle, P., Time domain characterization of micrometeorological data based on a two
691 sample variance. *Agricultural and Forest Meteorology* **2010,** *150*, (6), 832-840.
692 50. Burba, G., *Eddy covariance method for scientific, industrial, agricultural, and regulatory*
693 *applications: A field book on measuring scosystem gas exchange and areal emission rates*. LI-Cor
694 Biosciences: Lincoln, Nebraska, 2013; p 331.
695 51. Kaimal, J. C.; Finnigan, J. J., *Atmospheric Boundary Layer Flows: Their Structure and*
696 *Measurement*. Oxford University Press: Oxford, U.K., 1994.
697 52. Moore, C. J., Frequency response corrections for eddy correlation systems. *Boundary-*
698 *Layer Meteorology* **1986,** *37*, 17-35.
699 53. Pihlatie, M.; Rinne, J.; Ambus, P.; Pilegaard, K.; Dorsey, J. R.; Rannik, Ü.; Markkanen, T.;
700 Launiainen, S.; Vesala, T., Nitrous oxide emissions from a beech forest floor measured by eddy
701 covariance and soil enclosure techniques. *Biogeosciences* **2005,** *2*, (4), 377-387.
702 54. Pattey, E.; Edwards, G.; Strachan, I. B.; Desjardins, R. L.; Kaharabata, S.; Wagner Riddle,
703 C., Towards standards for measuring greenhouse gas fluxes from agricultural fields using
704 instrumented towers. *Canadian Journal of Soil Science* **2006,** *86*, (3), 373-400.
705 55. Gustin, M. S.; Ericksen, J. A.; Schorran, D. E.; Johnson, D. W.; Lindberg, S. E.; Coleman, J.
706 S., Application of Controlled Mesocosms for Understanding Mercury Air−Soil−Plant Exchange.
707 *Environmental Science & Technology* **2004,** *38*, (22), 6044-6050.
708 56. Engle, M. A.; Gustin, M. S.; Zhang, H., Quantifying natural source mercury emissions
709 from the Ivanhoe Mining District, north-central Nevada, USA. *Atmos Environ* **2001,** *35*, (23),
710 3987-3997.
711 57. Gustin, M. S.; Biester, H.; Kim, C. S., Investigation of the light-enhanced emission of
712 mercury from naturally enriched substrates. *Atmos Environ* **2002,** *36*, (20), 3241-3254.
713 58. Coolbaugh, M. F.; Gustin, M. S.; Rytuba, J. J., Annual emissions of mercury to the
714 atmosphere from natural sources in Nevada and California. *Environmental Geology* **2002,** *42*,
715 (4), 338-349.
716 59. Kuiken, T.; Gustin, M.; Zhang, H.; Lindberg, S.; Sedinger, B., Mercury emission from
717 terrestrial background surfaces in the eastern USA. II: Air/surface exchange of mercury within
718 forests from South Carolina to New England. *Applied Geochemistry* **2008,** *23*, (3), 356-368.
719 60. Kuiken, T.; Zhang, H.; Gustin, M.; Lindberg, S., Mercury emission from terrestrial
720 background surfaces in the eastern USA. Part I: Air/surface exchange of mercury within a
721 southeastern deciduous forest (Tennessee) over one year. *Applied Geochemistry* **2008,** *23*, (3),
722 345-355.
723 61. Gustin, M. S.; Engle, M.; Ericksen, J.; Lyman, S.; Stamenkovic, J.; Xin, M., Mercury
724 exchange between the atmosphere and low mercury containing substrates. *Applied*
725 *Geochemistry* **2006,** *21*, (11), 1913-1923.

726 62. Ericksen, J. A.; Gustin, M. S.; Xin, M.; Weisberg, P. J.; Fernandez, G. C. J., Air–soil
727 exchange of mercury from background soils in the United States. *Science of The Total*
728 *Environment* **2006,** *366*, (2–3), 851-863.
729 63. Nacht, D. M.; Gustin, M. S., Mercury Emissions from Background and Altered Geologic
730 Units Throughout Nevada. *Water, Air & Soil Pollution* **2004,** *151*, (1-4), 179-193.
731 64. Fritsche, J.; Wohlfahrt, G.; Ammann, C.; Zeeman, M.; Hammerle, A.; Obrist, D.; Alewell,
732 C., Summertime elemental mercury exchange of temperate grasslands on an ecosystem-scale.
733 *Atmos Chem Phys* **2008,** *8*, 7709-7722.

734

735

736 **For Table of Contents Only**

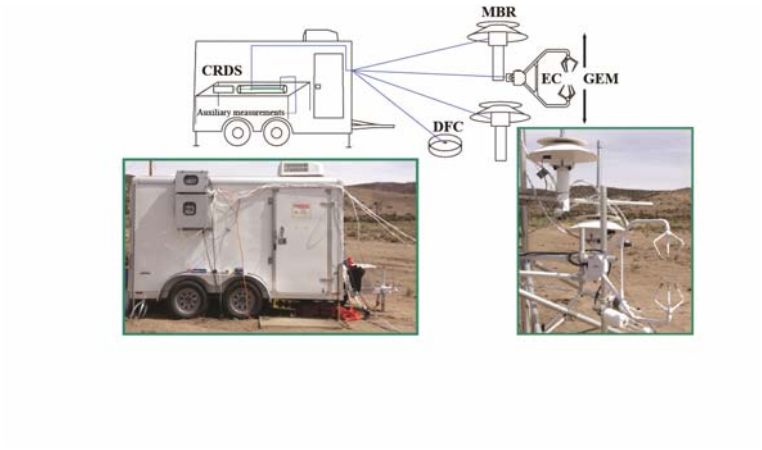

737

738

739

740